Cent. Eur. J. Geosci. • 5(4) • 2013 • 523-537
DOI: 10.2478/s13533-012-0151-6

VERSITA

Central European Journal of **Geosciences**

Geochemistry and geodynamics of the Mawat mafic complex in the Zagros Suture zone, northeast Iraq

Research Article

Hossein Azizi[1,2*], Ayten Hadi[3], Yoshihiro Asahara[4], Youssef Osman Mohammad[5]

1 *Mining Department, Faculty of Engineering, University of Kurdistan, Sanandaj, Iran,*

2 *Geology Department, Faculty of Basic Sciences, University of Tarbiate modares Tehran, Iran,*

3 *Department of Earth Science, College of Science, University of Baghdad, Bagdad, Iraq,*

4 *Department of Earth and Environmental Sciences, Graduate School of Environmental Studies, Nagoya University, Furo-cho, Chikusa, Nagoya 464-8601, Japan,*

5 *Department of Geology, College of Science Sulaimani University, Sulaimani, Iraq.*

Received 7 June 2013; accepted 17 September 2013

Abstract: The Iraqi Zagros Orogenic Belt includes two separate ophiolite belts, which extend along a northwest-southeast trend near the Iranian border. The outer belt shows ophiolite sequences and originated in the oceanic ridge or supra-subduction zone. The inner belt includes the Mawat complex, which is parallel to the outer belt and is separated by the Biston Avoraman block. The Mawat complex with zoning structures includes sedimentary rocks with mafic interbedded lava and tuff, and thick mafic and ultramafic rocks. This complex does not show a typical ophiolite sequences such as those in Penjween and Bulfat. The Mawat complex shows evidence of dynamic deformation during the Late Cretaceous. Geochemical data suggest that basic rocks have high MgO and are significantly depleted in LREE relative to HREE. In addition they show positive ε_{Nd} values (+5 to+8) and low 87Sr/86Sr ratios. The occurrence of some OIB type rocks, high Mg basaltic rocks and some intermediate compositions between these two indicate the evolution of the Mawat complex from primary and depleted source mantle. The absence of a typical ophiolite sequence and the presence of good compatibility of the source magma with magma extracted from the mantle plume suggests that a mantle plume from the D″ layer is more consistent as the source of this complex than the oceanic ridge or supra- subduction zone settings. Based on our proposed model the Mawat basin represents an extensional basin formed during the Late Paleozoic to younger along the Arabian passive margin oriented parallel to the Neo-Tethys oceanic ridge or spreading center. The Mawat extensional basin formed without creation of new oceanic basement. During the extension, huge volumes of mafic lava were intruded into this basin. This basin was squeezed between the Arabian Plate and Biston Avoraman block during the Late Cretaceous.

Keywords: Mawat complex • mantle plume • high Mg basalt • Zagros ophiolite • Iraq

*E-mail: Azizi1345@gmail.com

1. Introduction

Since the early Archean, mantle plumes have had an essential role in the development of the oceanic crust, continental rifting, hot spots and large igneous provinces [1, 2]. Mantle plumes are broadly envisaged to cause the upward movement of materials from the deeper parts of mantle accompanied by transfer of heat. Mantle plumes are hotter than the ambient mantle at shallower levels, and they have been widely invoked as the causes of intraplate magmatism. Partial melting may result from decompression of hotter material at shallower depths in the mantle [3–7] and extension of the lithosphere [8–10] or delamination of portions of the mantle lithosphere [11, 12]. Mantle plume melts directly interact with the depleted lithosphere causing partial melting at different depths. All these mechanisms are responsible for the development of different magma types such as; OIB, NMORB, EMORB and sometimes alkaline magma in different tectonic settings [13–19]. The northern and northeastern parts of Iraq are considered parts of the Zagros Orogenic Belt, which extends from southeast Turkey through northeast Iraq and northwest Iran to northern Oman. Several structural classifications of Iraq have been proposed. [20] classified the Iraqi Zagros Belt into three structural units: the outer stratigraphically lowest (Naupurdan) unit of flysch-like sediments; the middle volcano-sedimentary (Walash) unit and the inner stratigraphically highest (Qandil series) unit. [21] Classification is based on the plate tectonic theory is the most recent classification of Iraq . According to this classification, Iraq is divided into three main tectonic zones: (1) the Stable Shelf including the central and western parts of Iraq; (2) the Unstable Shelf with four subzones, including the northern and east-central part of Iraq, which are characterized by structural trends parallel to the Taurus-Zagros Suture Zone; and (3) the Suture Zone which extends through the extreme northeast of Iraq and comprises three major parts: the Qulqula-Khwakurk, the Penjween-Walash, and the Shalair zone. The Iraqi Zagros Suture Zone was formed within the Neo-Tethys ocean and then thrust over the Arabian Plate in the Late Cretaceous obduction, followed by collision during the Miocene-Pliocene. The Penjween-Walash Zone represents the main central Neo-Tethys, forming a continuous belt that extends along the Iraq-Iran border and has been thrusted over the Qulqula-Khwakurk Zone [21–24]. This zone comprises volcano-sedimentary sequences, which formed during the Cretaceous ocean spreading in the Neo-Tethys, as well as Paleocene arc volcanic- mafic and ultramafic intrusions, which were emplaced during the final closure of the Neo-Tethys Ocean. The Penjween-Walash Zone constitutes three thrust sheets: the structurally lowest Naupurdan, the middle Walash and the upper Qandil Eocene-Oligocene series [43]. The upper Qandil contains mafic and ultramafic massifs represented by Mawat, Penjween, Bulfat and Pushtashan [23]. The Shalair Zone is the structurally highest thrust sheet in Iraq and it is considered an integral part of the Sanandaj-Sirjan Zone of Iran [25] within the extreme northeast of Iraq. This zone is the inner-most metamorphosed unit of the Upper Permian overlain by Jurassic and Lower- Cretaceous fore-arc meta-sediments and Upper Cretaceous calc- alkaline andesite (Kata Rash unit) with imbricates of the Upper Triassic deep water carbonates.

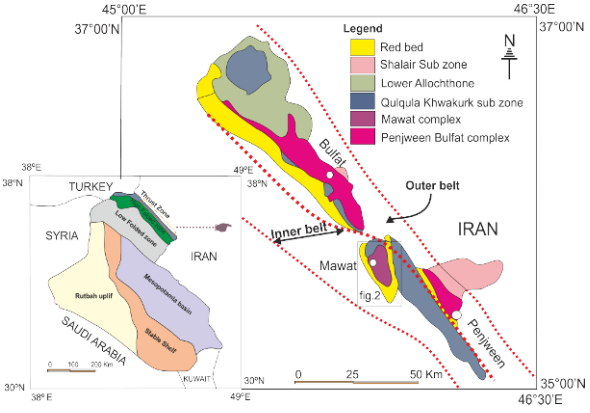

Figure 1. The distribution of mafic and ultramafic rocks [51] as two parallel belts in the northeast of Iraq extending in a northwest-southeast direction. The inner Mawat group and the outer Penjween-Boulfat, which extends to the Iranian border. These belts are separated by the Qulqula-Kuwakurk subzone. The inset map is the Geological map of Iraq [66] which shows the main structures in Iraq.

The Mawat area is located in the northeast of Iraq (Fig.1) near the Iranian border and is mainly composed of mafic rocks with minor ultramafic rocks. This complex does not show a typical ophiolite sequence, but has some affinity to an ophiolite complex, therefore most researchers have considered it as an ophiolite complex comprising a remnant of Neo-Tethys oceanic crust in the Zagros Suture Zone. The goal of the study is to investigate the geochemical affinities of the Mawat Complex in order to develop a model for its petrogenesis based on the chemical and isotopic data and to suggest a new scenario based on a proposed mantle plume along the Arabian passive margin during the formation of Neo-Tethys oceanic crust between the Arabian and Iranian Plates.

2. Regional geology

The Cretaceous Mawat complex (Fig. 2) covers an area of about 250 square kilometers [22, 26] and as mentioned

is a part of Penjween- Walash Zone [21]. This complex is situated between two thrust sheets from the east and the west with NW-SE trend. The western thrust sheet is the Naopurdan Formation, which is composed of sedimentary sequences of Eocene-Oligocene limestone. The eastern sheet is a complex sequence of regionally metamorphosed red shale, limestone, and metamorphosed mafic volcanic and intrusive bodies. This sheet is correlated with the Walash Volcanic Series of Eocene age [22, 27] The Naopurdan and Walash sheets generally overlie some flysch sediments of Upper Cretaceous age (Shiranish, Aqra, and Tanjero Formations). The outcrops of the Mawat complex observed in the field include the following successions from the upper to lower stratigraphic levels: Recrystallized limestone with interlayered mafic tuff are observed in the upper part (Fig. 2) suggesting a submarine origin for this complex. The mafic rocks are the main components of the intrusive bodies and include gabbro and basaltic rocks, which extend for about 250 square kilometers. These rocks are the main subject of this paper. The separation of these rocks into different groups is difficult, because in most cases they are deformed and mixed with sediments and are also largely covered by farmland. In the lower (western) parts they over-thrust the younger Tertiary red beds sediments (Fig. 2). In general, dynamic deformation has affected the entire Mawat complex, with different strain rates in the brittle and ductile zones, and as a result the rocks mainly have a mylonitic fabric. In the ductile zone high-grade shearing has produced sheath folds and isoclinal folds, stretched lineation and boudinage (Fig. 3. a, b, c and d), although some mylonitic foliation is found to surround some less deformed parts (Fig. 3 f, g). In the low strain domains there are relict gabbroic textures that have been surrounded by mylonitic foliation (Fig. 3 g and h). In the southwest of the complex there is well-developed sigmoidal boudinage with C planes that may be mistaken for pillow structures (Fig.3 h). Brittle zones are developed in the rim of the Mawat complex, where the rocks have been crushed without mylonitic foliation (Fig. 3 i and J). On the other hand, within the central part, some un-deformed gabbroic rocks occur. Our field observations indicate that mylonitic gabbros and volcanic rocks, deformed in the shear zone at low to intermediate metamorphic grade, are the main components; hence, dynamic deformation is responsible for Mawat metamorphism.

The ultramafic rocks extensively overthrust the mafic rocks (Fig. 2). They comprise dunite, harzburgite and pyroxenite. At the base, in contact with the mafic rocks, they are deformed and crushed. Outcrops of ultramafic rocks at the Mawat Complex are much less common than at other complexes such as the Penjween or those of the Zagros ophiolite in Iran, e.g. in the Kermanshah and Khoy area

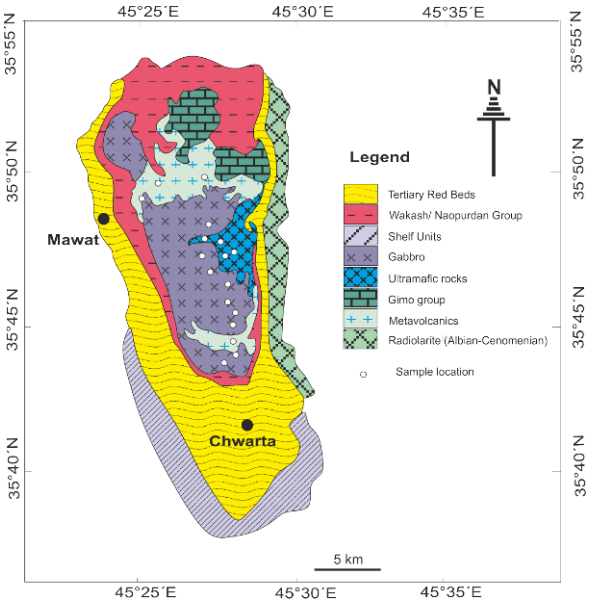

Figure 2. Modified geological map of Mawat [22]. Rectangles show locations of samples under study.

where the main body of the ophiolite complex comprises ultramafic rocks [28–31]. Mawat ultramafics show false bedding because of parallel fractures (Fig. 4 a and b), and are variably serpentinized [32] and rich in chromite pods 32, 33. The harzburgite and dunite are cut by some fresh clinopyroxene dykes (Fig. 4 c). In addition, there are some metavolcanic rocks representing either tuff or lava layers, interbedded with some marble layers in the west and northwest of this complex (Fig. 4 d, e and f). The Mawat complex is overlain by the Gimo group, which is composed of marble and volcanic rocks. Late stage granitic dykes cut the complex.

3. Petrography

Petrographic study of the mafic rocks shows that most of these rocks have been deformed. As mentioned in the geological background, the main fabrics are mylonite, protomylonite and less frequently ultra-mylonite. The dominant mineral is clinopyroxene, partially altered to chlorite+tremolite+actinotile. After pyroxene, the next most abundant phase is plagioclase, some of which is altered to calcite+epidote+albite. These rocks show porphyroclastic texture with large pyroxenes as well as secondary amphibole and plagioclase phenocrysts. The effect of dynamic deformation on these rocks is obvious from the appearance of shear structures such as S-C planes, mica fish, stretching lineation and isoclinal and sheath folds

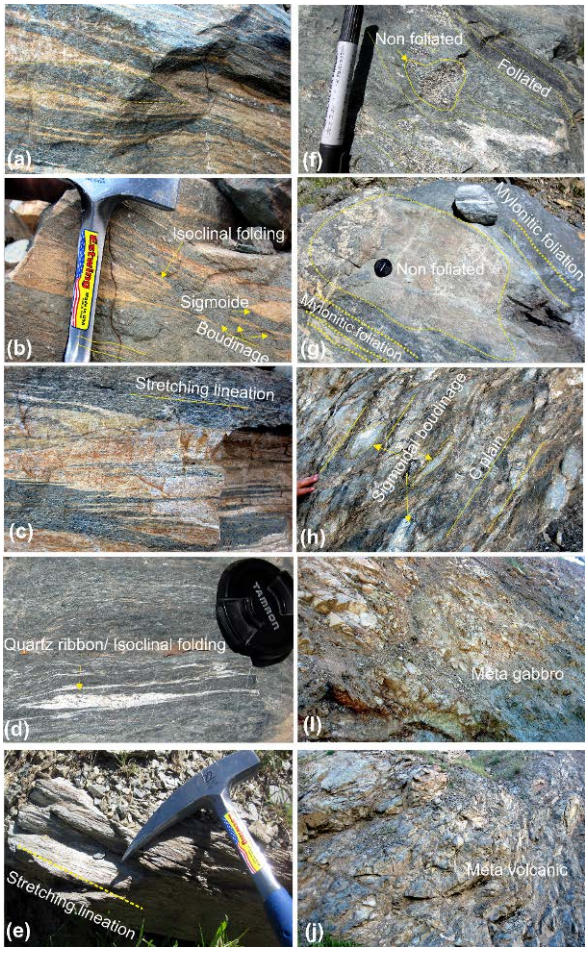

Figure 3. Field structures of Mawat igneous complex: Mylonitic structures such as sheath and isoclinal folds, sigmoid, boudinage structures and stretching lineation [67]. These structures suggest the ductile deformation occurred at high strain rates and moderate temperatures (a, b, c, d and e). Conservation of some undeformed parts between the mylonitic foliation (f, g), sigmoidal boudinage in metavolcanics (h) and brittle deformation in the gabbroic and volcanic rocks, which reflects deformation at low temperatures without formation of mylonitic foliation (i, j).

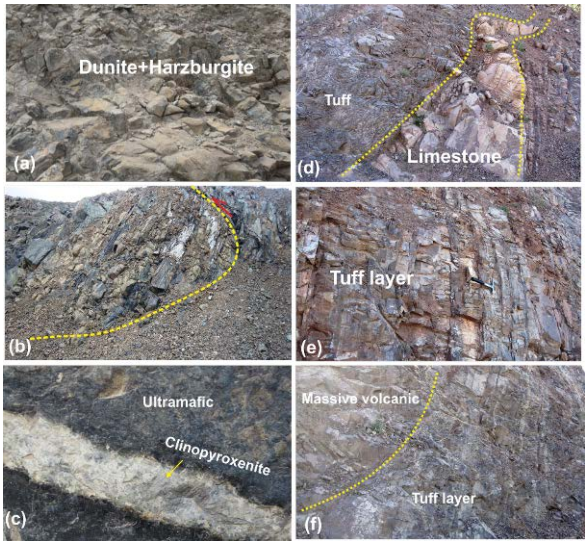

Figure 4. Ultramafic rocks show some parallel fractures, which are cut by clinopyroxenite dykes (a, b and c respectively). In the rim and upper parts of the mafic rocks, probably in the Gimo Group, some mafic tuff layers are interbedded with marble layers (d). The metavolcanics are observed as tuff and compact lava (c, d).

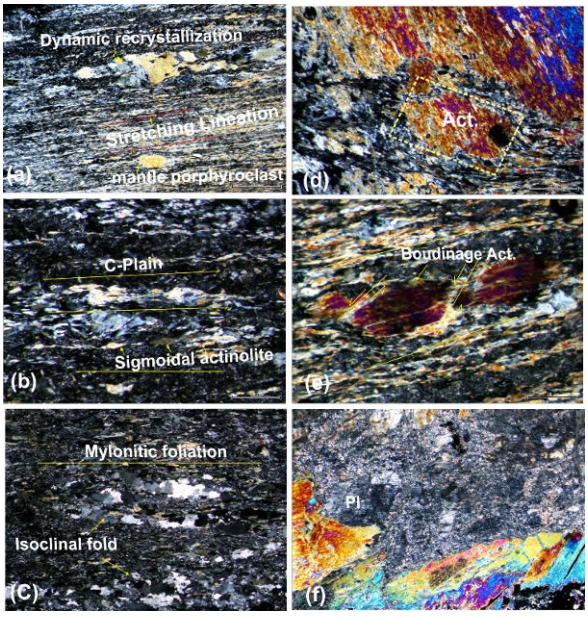

Figure 5. Photomicrograph showing the main textural features. The microscopic textures confirm the field observations of different deformational structures. This photo shows the ductile and brittle deformation of this complex; Dynamic recrystallization in the amphiboles parallel to the stretching lineation(a); formation of S-C plain fabric (b) and isoclinal folding in quartz ribbons(c); deformed clinopyroxene as mantle porphyorclasts and formation of mylonitic foliation between them (d); antithetic, rhombohedral fragments and boudinate pyroxene minerals (e); brittle deformation in plagioclase fragment without formation of the mylonitic foliation (f).

(Fig. 5 a and b). In addition, the sigmoidal shape of actinolite between the shear bands, the isoclinal folds in the quartz ribbon and the mica fish structure in actinolite developed with mylonitic foliation (Fig. 5 d, e). Also, some plagioclases and some relict clinopyroxenes show brittle deformation in the low strain area. Finding fresh samples in these rocks is difficult, but some relict parts show the granular and porphyritic textures that indicate source mafic volcano-plutonic rocks such gabbro and basalt. The modal classification of these rocks is somewhat difficult because of significan deformation and alteration to metamorphic minerals. Dynamic structures and fabrics as well as mineral paragenesis suggest that metamorphism has

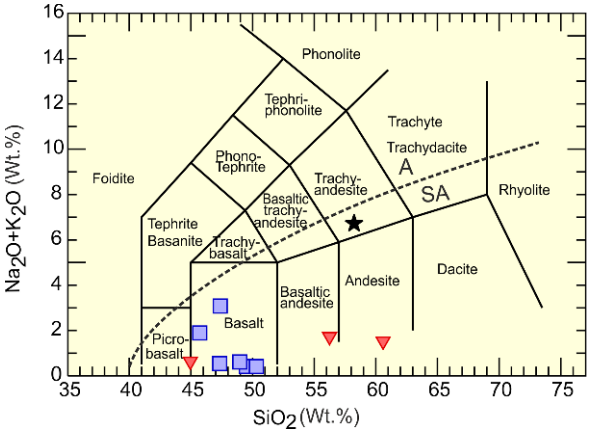

Figure 6. Chemical classification based on [35] diagram. The Mawat mafic rocks are plotted in the basalt and basaltic andesite fields. All samples plot in the sub-alkaline field with low Na_2O+K_2O (Wt. %). *Filled rectangles represents the high magnesium basalt (HMB), filled triangles are for the second group and black stars are for the third volcanic group. A=Alkaline and SA=Sub alkaline.*

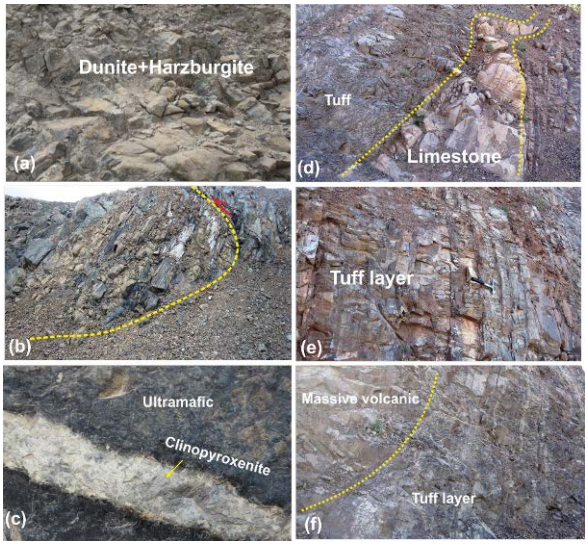

Figure 7. Primitive mantle, NMORB, and OIB- normalized REE patterns [36] for the three mafic-intermediate (HMB, second, and third) groups of Mawat, (a, b and c respectively). The REE patterns for these rocks show different trends. REE normalized with primitive mantle for the ultramafic rocks indicates the REE-depleted nature of these rocks (d).

occurred in the shear zone of low to medium grades of green schist to lower amphibolite facies, resulting in the formation of some high grade structures such as mylonitic fabric in this complex. The ultramafic rocks are completely deformed and show the tectonite structures. They are mantle ultramafics with no evidence of cumulate texture (which would suggest crystallization from the mafic magma in a magma chamber). The ultramafic rocks are classified into three groups: the first is dunite, which is composed mainly of fresh olivine, some of which show serpentine minerals around the rims and within fractures. Previous studies [32] have shown that the serpentine in these rocks is mostly chrysotile that formed at high temperature. Kink and deformation bands appear in dunite with disseminated chromite. The chromite is observed as black coarse grains on the macroscopic and microscopic scale. Harzburgite is the second group of ultramafic rocks in this area and is composed of orthopyroxene and olivine with chromite. Some orthopyroxenes are fresh and some are replaced by bastite, whilst some of the olivine grains are partially replaced by serpentine. Clinopyroxenite dykes which cut the ultramafic rocks are composed mainly of fresh clinopyroxenes with some grains partially altered along the cleavage planes to secondary amphiboles. The late-stage felsic granitic dykes are composed of alkali feldspars, quartz, muscovite and tourmaline and show coarse grain granular texture.

4. Analytical technique

Following the study of thin sections, several samples were chosen for whole-rock chemical analysis. An XRF Rigako machine (Nagoya University, Japan) was used for analyses of the major elements. For chemical analyses 0.70 g sample plus 6.0 g lithium tetra- borate after was used. Each sample was melted at a temperature of 1050°C for 15 to 25 minutes. In some cases, in order to produce a homogeneous glass bead the melting was repeated two or three times. Losses on ignition (LOI) were calculated by weight difference after ignition at temperature of 950°C. 100 to 200 mg of powder of the homogenized samples was then decomposed in 3 ml HF (50%) and 0.5 to 1 ml $HClO_4$ in a covered Teflon beaker, at a temperature range of 120-140°C on a hot plate in a clean room. After 72 hours the cover was removed and the samples were dried on a hot plate at 140°C under an infrared lamp for 24 to 48 hours to make sure that the samples were completely dry. The second step involved dissolving the dried samples in 10 ml HCl 2.4 normal . After centrifuging the solution, the residue was transferred to small Teflon beakers and the dissolved solution was kept in these clean Teflon beakers. After drying the residue on a hot plate 1.5 ml concentrated HF and 0.5 ml concentrated $HClO_4$ were added .The small Teflon beakers were then put inside the jacket steel bomb in the oven at 180°C for 3-5 days until the restite minerals were completely dissolved. Finally, after

cooling, these solutions were mixed with the previous dissolved solutions. The dissolved samples were dried again on the hot plate at 100 to 120°C with infra-red lamps. After drying, the samples were dissolved in 10 ml HCl of 2.0 molar and the resulting solutions were divided in to three parts at the ratio 3:1:1 for Sr-Nd isotopes and REE, 1 part for isotope dilution and 1 part for trace elements. Then, all samples were dried on the hot plate under infrared light. For trace elements concentration measurement the following procedure used: After drying, the samples were diluted in 16ml HNO_3 (2%) in order to maintain consistency with our ICP-MS standard calibration, using standard solutions for the elements of the interest, ranging in concentration from 0.02 to 30 ppb. We diluted the samples with HNO_3 (2%) again in the measuring bottles using 0.25 to 0.5 mg of sample solution and 10 mg HNO_3 (2%). The mixed solution could then be measured with ICP-MS. After drying the solution, an HCl ion exchange column was used to collect the Sr and REE. The REE solutions were divided into 1:10 parts for REE and natural Nd isotopes. The REE solutions were dried on the hot plate at low temperature under an infrared lamp. Dried samples were dissolved in 0.5ml concentrated HNO_3. To exclude Ba, the HNO3 ion exchange column was used. The final solutions were dried and dissolved in 10ml HNO_3 (2%), then diluted to around 1/10th with HNO_3 (2%). The ICP-MS Agilent 7700 Mass Hunter was used for trace and REE analyses in this project. For solutions an internal standard is needed and so the concentrations of elements were measured in two different conditions: Argon and no gas. Finally, the low RSD was used for calculation of the concentration of elements. The error in the ICP-MS based on the factory brochure is less than 5% and extended to 3%. For the natural isotope analyses of Sr and Nd, 100-200 ng Sr with 2 M H3PO4 was loaded on a Ta single filament and 100-200 ng Nd on a Re triple filament. Procedure blanks are 19.52 ng for Rb, 3.07 ng for Sr, approximately 0.4 ng for Nd, and approximately 0.06 ng for Sm. Sr and Nd isotope ratios were measured using a thermal ionization mass spectrometer (TIMS), VG Sector 54-30, at Nagoya University, Japan. The mass fractionation during the Sr and Nd isotope measurements is corrected based on 86Sr/88Sr = 0.1194 and 146Nd/144Nd = 0.7219. The isotope abundances of Rb, Sr, Nd, and Sm based on the ID method were measured with a thermal ionization-quadruple mass spectrometer (Finnigan MAT Thermoquad THQ) at Nagoya University. In this work, NBS-987 and JNdi-1 [34] were adopted as the natural Sr and Nd isotope ratio standards, respectively.

5. Geochemistry

5.1. Mafic group

The results of the chemical analyses are listed in table 1. Chemical data from some less altered and fresh samples show that the Mawat volcano-plutonic complexes are rich in MgO and CaO, while depleted in K_2O+Na_2O and TiO_2. An important characteristic of the Mawat complex is the low values of TiO_2 (<0.5%) as compared to MORB and back arc basin basalts (BABB). Also these data show that Mawat is not a simple igneous complex. It can be separated into three different groups: the first group comprises the main body of this complex and we call it high Mg basalt (HMB). The second most abundant group after the HMB is the basalts and andesites. The third group has outcrops as tuffacious layers between the sedimentary bands of limestone and chert to the north and west of the complex. Geochemical data do not show continuous trends between these three groups (Harker diagram not shown). Plotting the data on classical diagrams such as the Le Bas et al [35] diagram showed that these samples fall in the basalt, andesitic basalt and trachy-andesite fields (Fig. 6). Also this diagram shows that all samples plot in the sub-alkaline field and are characterized by low alkali elements (Na_2O+K_2O <2%). The amount of TiO_2 is low (Table1) in comparison with other MORB examples such as the Atlantic, Pacific and Indian oceanic basalts (1.32, 1.66, and 1.22% respectively; Georock references data base). Also the Mg number (Mg#) is variable between 73 to 85 and 36 to 73 and 67 for HMB, in the second and third groups respectively. The second group has some affinity with NMORB (Table 1). The HMB rocks also have variable amounts of Al_2O_3 and CaO which range from 12-25 Wt. % and 7-16 Wt. % respectively. These values are much higher than those of normal oceanic basalt whereas Fe_2O_3 contents are much lower than that of normal oceanic basalts. REE patterns normalized to Primitive mantle (PM), NMORB and OIB respectively (normalization values after [36]) are shown in Fig.7 a, b and c respectively. These patterns suggest differences in trends in the three groups. Positive trends are clear in the second group from the LREE to HREE with different slopes. The HMB rocks show much depleted REE compared with NMORB and OIB, but the second group shows some affinity with NMORB and to lesser extend with OIB. The third group shows a different trend from the two other groups, characterized by a negative trend from the LREE to HREE with a low gradient. For discrimination of the magma type we have used the ΔNb according to the following formula: ΔNb=[1.72+Log (Nb/Y)-1.92Log(Zr/Y)] [37]. The calculated ΔNb values (Table.1) for both HMB and the second group are positive and vary from 1 to 3 and 2-3 for HMB

and second group rocks respectively, whereas the third group shows negative values (-0.2). The positive ?Nb values confirm OIB- type magma, because ΔNb in MORB type magma is generally less than zero [37]. Data from the GeoRock database confirm that the ΔNb values for Atlantic, Pacific and Indian oceanic crust are negative. In the Nb/Yb versus the Th/Yb ratios diagram [38] these samples show positive trends and all are plotted within the mantle array (Fig. 8 a). The HMB samples are plotted close to MORB and extend to the OIB [39]. On Nb/U versus the Nb diagram (Fig. 8-b) the HMB are characterized by high Nb/U ratios and high Nb and all have plotted outside the MORB and OIB fields. The second group is extended to the MORB and OIB field whereas the third group differs from these two and falls in MORB and arc fields. This indicates that the three groups of rock have high Nb value. On Pb versus Pb/Ce diagram (Fig. 8 c) [39], the second and third groups plot at near the OIB field but HMB is different and shows the high Pb and Pb/Ce ratios values (1-100). This probably reflects some contamination with continental sediments, but this must be taken with caution because the behavior of the other elements does not confirm the effect of contamination with continental materials [40]. Also on the La/Nb versus Ba/Nb diagram [39] these rocks show positive trends (Fig. 8-d), but the values of La/Nb ratios for HMB group are much lower than MORB and OIB, where the second and third groups are plotted near OIB and arc fields.

5.2. Ultramafic rocks.

The ultramafic rocks show low SiO_2 content ranging from 39 to 41 Wt. % with a higher percentage of SiO_2 in the clinpyroxenite dyke (53.10 Wt. %) (Table 1). High values of MgO (45 Wt. %), and low values of Al_2O_3 and CaO (less than 0.3 Wt. % and o.7 Wt. % respectively), indicate that there is no, or very rare, clinopyroxene in these rocks. Field, petrographic observations and chemical data demonstrate that these ultramafic rocks are harzburgite and dunite. In addition, they are rich in Cr (1827-4906 ppm) and Ni (501-2736ppm). These rocks are much depleted in REE and the total REE is less than 1 (Table 1), which suggests that these rocks have not been metasomatized by OIB-type magma or slab-derived fluids.

Table 1: Chemical compositions of the Mawat complex.

Sample		IQ-MK1	IQ-MK4	IQ-MK5	IQ-MK6	IQ-MK7	IQ-MK8	IQ-MK2	IQ-MK9	IQ-MK10	IQ-MVT1	IQ-MU1	IQ-MU2	IQ-MU3	IQ-MU4	IQ-MLGD1
Rock type		Basalt	Gabbro	Gabbro	Gabbro	Gabbro	Gabbro	Basalt	Andesite	Andesite	Trachy andesite	Harzburgite	Harzburgite	Dunite	Clinopyroxenite	granite
Group		HMB	HMB	HMB	HMB	HMB	HMB	Group 2	Group 2	Group 2	Group 3	ultramafic	ultramafic	ultramafic	ultramafic	
SiO2	Wt%	47.38	47.34	49.49	48.97	50.31	45.72	44.96	60.59	56.25	58.24	41.80	40.64	39.71	53.10	66.76
TiO2	Wt%	0.46	0.13	0.10	0.11	0.07	0.04	0.09	0.82	0.55	0.40	0.00	0.00	0.00	0.04	0.06
Al2O3	Wt%	16.9	16.9	16.8	15.4	12.8	25.5	18.0	13.3	14.8	16.0	0.2	0.3	0.1	1.0	19.6
Fe2O3	Wt%	6.54	6.35	6.89	7.35	4.02	3.04	6.83	11.94	9.79	4.95	9.58	8.18	10.14	3.52	0.60
MnO	Wt%	0.14	0.12	0.13	0.15	0.09	0.07	0.10	0.18	0.19	0.07	0.14	0.12	0.14	0.08	0.02
MgO	Wt%	9.3	11.0	10.6	11.8	12.3	6.3	10.8	3.5	5.7	5.3	43.7	44.7	48.3	20.5	0.5
CaO	Wt%	13.1	16.0	15.0	14.6	19.2	14.8	16.1	7.5	10.2	4.3	0.7	0.4	0.4	20.3	0.6
Na2O	Wt%	2.1	0.5	0.4	0.6	0.4	1.0	0.6	1.5	1.6	5.6	0.1	0.1	0.2	0.2	11.5
K2O	Wt%	0.98	0.038	0.013	0.011	0.007	0.891	0.038	0.035	0.125	1.117	0.003	0.006	0.002	0.006	0.10
P2O5	Wt%	0.02	0.008	0.007	0.006	0.005	0.006	0.009	0.061	0.047	0.111	0.005	0.006	0.005	0.005	0.12
LOI	Wt%	3.34	1.66	0.57	0.94	0.74	2.65	2.55	0.46	0.80	3.88	3.83	5.82	1.10	1.30	0.11
Total		100.1	100.0	100.0	100.0	100.0	100.0	100.1	100.0	100.0	99.9	100.0	100.2	100.0	100.0	100.0
V	ppm	138.6	178.3	193.3	183.0	174.5	57.4	12.6	264.6	277.7	86.9	33.7	21.5	27.9	177.8	2.4
Cr	ppm	266.0	244.7	285.4	463.3	552.2	320.6	18.0	20.2	34.7	179.0	3532	2430	4906	1827	12.1
Co	ppm	34.4	39.9	40.9	44.5	28.2	19.6	9.0	31.4	33.8	19.7	117	116	133	39	1.4
Ni	ppm	75.2	144.6	96.1	120.8	122.9	82.2	4.6	13.0	38.6	104.2	2114	2550	2736	501	10.7
Cu	ppm	6.4	115.2	4.1	31.9	2.2	49.0	12.4	51.4	55.1	33.5	28.0	3.6	2.3	33.3	2.7
Zn	ppm	73.7	71.9	39.8	45.5	28.9	18.5	65.7	62.4	79.1	63.8	55.7	44.6	57.5	19.0	13.9
Ga	ppm	10.54	10.2	10.4	9.4	7.0	13.07	12.9	13.2	13.9	17.6	0.63	0.52	0.66	1.23	17.0
Rb	ppm	25.44	0.6	0.3	0.3	0.3	12.23	0.8	0.5	1.0	10.0	0.58	0.40	0.15	0.14	1.8
Sr	ppm	404.1	93.6	81.8	63.3	114.7	213.7	92.9	130.9	158.5	524.7	1.2	1.0	0.8	5.2	207.5
Zr	ppm	4.6	4.5	1.9	1.3	2.5	1.5	1.4	6.7	2.8	66.0	14.4	0.5	1.4	0.3	6.8
N b	ppm	1.2	5.5	3.5	1.0	1.4	0.9	3.5	6.2	2.0	5.2	20.6	2.9	4.5	0.7	10.0
Cs	ppm	5.0	0.2	0.1	0.1	0.3	1.4	0.1	0.1	0.3	0.3	0.1	0.0	0.0	0.0	0.1
Ba	ppm	51.2	4.1	4.9	1.4	2.0	15.2	6.8	9.6	20.5	87.5	0.6	1.2	0.3	0.8	19.1

Pb	ppm	1.25	0.67	1.31	24.39	0.58	4.04	0.68	0.84	1.33	2.06	0.47	0.48	0.30	0.45	2.37
Th	ppm	0.08	0.22	0.08	0.01	0.06	0.05	0.39	0.43	0.23	1.35	2.10	0.09	0.22	0.02	4.28
U	ppm	0.04	0.01	0.00	0.00	0.01	0.00	0.11	0.10	0.10	0.32	0.03	0.00	0.00	0.00	6.52
Ta	ppm	0.11	0.15	0.14	0.01	0.10	0.05	0.02	0.30	0.04	0.27	0.26	0.01	0.46	0.06	0.58
Y	ppm	3.76	4.11	2.50	2.67	2.01	1.04	24.51	19.96	24.23	7.73	0.00	0.00	0.00	0.01	10.74
La	ppm	0.30	0.15	0.06	0.06	0.08	0.07	1.76	1.32	1.50	7.06	*n.d	n.d	n.d	n.d	5.13
Ce	ppm	0.81	0.46	0.19	0.18	0.22	0.18	5.08	4.36	4.95	14.83	n.d	n.d	n.d	n.d	11.46
Pr	ppm	0.12	0.08	0.04	0.04	0.03	0.03	0.77	0.74	0.81	1.89	n.d	n.d	n.d	n.d	1.32
Nd	ppm	0.68	0.53	0.25	0.27	0.21	0.17	4.42	4.21	4.77	7.63	n.d	n.d	n.d	n.d	4.46
Sm	ppm	0.28	0.27	0.14	0.15	0.10	0.07	1.73	1.67	1.74	1.27	n.d	n.d	n.d	n.d	1.08
Eu	ppm	0.15	0.14	0.12	0.11	0.06	0.10	0.62	0.62	0.55	0.43	n.d	n.d	n.d	n.d	0.13
Gd	ppm	0.43	0.48	0.27	0.30	0.20	0.12	2.76	2.46	2.81	1.39	n.d	n.d	n.d	n.d	1.15
Tb	ppm	0.09	0.10	0.06	0.06	0.04	0.02	0.57	0.50	0.57	0.23	n.d	n.d	n.d	n.d	0.27
Dy	ppm	0.67	0.76	0.45	0.48	0.35	0.18	4.16	3.55	4.16	1.48	n.d	n.d	n.d	n.d	1.79
Ho	ppm	0.15	0.17	0.10	0.11	0.08	0.04	0.95	0.79	0.95	0.30	n.d	n.d	n.d	n.d	0.35
Er	ppm	0.47	0.51	0.32	0.34	0.26	0.13	2.97	2.42	2.89	0.84	n.d	n.d	n.d	n.d	1.07
Tm	ppm	0.07	0.07	0.05	0.05	0.04	0.02	0.44	0.35	0.43	0.12	n.d	n.d	n.d	n.d	0.17
Yb	ppm	0.48	0.50	0.33	0.34	0.28	0.13	3.03	2.37	2.95	0.77	n.d	n.d	n.d	n.d	1.17
Lu	ppm	0.07	0.08	0.05	0.05	0.04	0.02	0.45	0.34	0.43	0.12	n.d	n.d	n.d	n.d	0.16
ΣREE		4.75	4.31	2.44	2.54	1.98	1.28	29.73	25.71	29.53	38.34					29.70
Mg#		73.7	77.4	75.4	76.1	85.8	80.4	75.8	36.8	53.5	67.9	90.0	91.5	90.4	92.0	63.09
ΔNb		1.0	1.8	2.1	1.9	1.4	1.4	3.3	2.1	2.4	-0.2					

Mg#=100*[MgO]/([MgO]+[FeOt])
ΔNb=[1.72+Log(Nb/Y)-1.92Log(Zr/Y)](Fitton *et al.*, 1997).
*nd=not determined

5.3. Granitic dyke

The felsic granitic dykes are characterized by high SiO_2 and Al_2O_3 (Table-1) and generally are of peraluminous S-type granite.

6. Sr-Nd Isotopes

The $^{87}Sr/^{86}Sr$ and $^{143}Nd/^{144}Nd$ ratios are almost the same for all mafic rocks, with small differences (Table 2). The $^{87}Sr/^{86}Sr$ initial ratios calculated based on variation of the $^{87}Rb/^{86}Sr$ versus $^{87}Sr/^{86}Sr$ ratios are: 0.7044 and 0.7051 for the HMB and the second group respectively (Fig. 9a and b). For the third group of mafic rocks this value is 0.7055. All groups have low $^{87}Rb/^{86}Sr$ ratio, at less than 0. 2 and 0.03 in the HMB and second group respectively (Table 2). Plotting $^{87}Sr/^{86}Sr$ versus $^{143}Nd/^{144}Nd$ shows that the mafic rock assemblages fall within the depleted mantle field (Fig. 9-c), with a negative trend between the $^{143}Nd/^{144}Nd$ and 87Sr/86Sr ratios. The calculated εNd values for all three groups range from +5 to +8 while the εSr values range from -3 to +17. This indicates a depleted mantle source for Mawat mafic rocks. Plotting the three mafic groups on the $^{87}Sr/^{86}Sr$- $^{143}Nd/^{144}Nd$ ratio diagram suggests a mixing trend between these three groups (Fig.9-d). Group 2 samples are plotted between the HMB and third volcanic groups but are much closer to the third group (Fig. 9- d).

7. Discussion

The Zagros ophiolites extend as two separated parallel belts with NW-SE trends between the Arabian and Iranian Plates. In the northeast of Iraq these two are separated by the Biston Avoraman Block (BAB) with Triassic to Jurassic deep marine sediments (Fig. 10). Outer ophiolite zones such as Pejnween and Bulfat (Fig. 2) show a complete ophiolite sequence, comprised of pillow lava, sheeted dykes and layered gabbro and show good correlation with the Iran Zagros ophiolite [41–43]. [44] proposed this complex as a suture zone between the Arabian and Iranian Plates. The Mawat complex has been considered as an inner belt and as a part of an inner ophiolite belt which have been generated in the mid-oceanic ridge, island arc or supra-subduction zone settings [22, 24, 26, 27, 33, 45–53]. [54] proposed an extensional tectonic regime during the Triassic to Jurassic and a compressional regime throughout the Cretaceous and Tertiary in this area. [55] considered the Mawat - Chwarta areas as a graben basin that has formed by subsidence attributed to the normal faulting. [21] considered the Mawat complex to be different in lithology and sequence to the Penjween complex and considered a completeophiolite sequence to be abasent. Our findings do not support a typical ophio-

Table 2. Sr and Nd isotope ratios for whole rocks and minerals for the granitic dyke (IQ-MLG2) sample.

Sample name	$^{87}Rb/^{86}Sr(p)$	±2SE	$^{143}Nd/^{144}Nd(p)$	±2SE	$^{87}Rb/^{86}$	ε^0 Sr	ε^0Nd
IQ-MK1	0.70574	0.000014	0.512940	0.000049	0.155	17.6	5.9
IQ-MK2	0.70537	0.000016	0.512953	0.000026	0.012	12.4	6.1
IQ-MK4	0.70430	0.000014	0.513047	0.000022	0.003	-2.9	8.0
IQ-MK5	0.70428	0.000014	0.513014	0.000029		-3.1	7.3
IQ-MK6	0.70398	0.000015	0.513109	0.000097	0.006	-7.4	9.2
IQ-MK7	0.70524	0.000014	0.512928	0.000029		10.5	5.7
IQ-MK8	0.70521	0.000016			0.140	10.0	
IQ-MK9	0.70525	0.000014	0.512972	0.000009		10.6	6.5
IQ-MK10	0.70525	0.000016	0.512991	0.000017	0.012	10.6	6.9
IQ-MVT1	0.70557	0.000014	0.512934	0.000008	0.048	15.2	5.8
Mineral isochron							
Plagioclase-MLGD2	0.70440	0.000015			0.025		
Whole rock-MLGD2	0.79110	0.000013	0.512949	0.000009	48.29		
Muscovite-MLGD2	4.475779	0.000071			2833.3		

The Nd and Sr natural ratios were normalized based on $^{146}Nd/^{144}Nd$=0.7219 and $^{87}Sr/^{87}Sr/^{86}Sr$=0.1194
Average and 1σstandards samples for JNdi-1=0.512097±0.000010(n-12) and for NBS_{987}=0.71024±0.00001 (n=17).
CHUR(chondritic Uniform Reservoir) values $^{147}Sm/^{144}Nd$=0.1967 and $^{143}Nd/^{144}Nd$=0.512638, were used to calculate ε^0
JG-1a ad reference sample was measured as the follows:
$^{87}Sr/^{86}Sr$ 0.710980±8(2σ),Rb=172.63ppm, Sr=188.87, Np=18.48 and Sm=4.68 ppm
$\varsigma^0Nd=((^{143}Nd/^{144}Nd)^P_{sample}/(^{143}Nd/^{144}Nd)^)_{CHUR})) - 1)*10000$

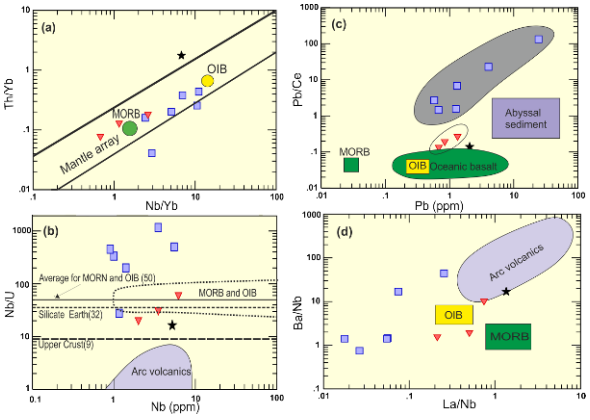

Figure 8. Nb/Yb-Th/Yb diagram of [38], (a): Most of the samples for the mafic rocks of the three groups are plotted in the mantle array, near the MORB and OIB fields. (b): Nb-Nb/U diagram: the HMB group rocks are completely different and plot above the MORB area with high Nb/U ratios. Most of the rocks of the second group plot near the MORB and OIB, whereas the rocks of the third group extend to calc-alkaline area. (c) Pb- Pb/Ce diagram, HMB samples show depletion in Ce as compared with the two other groups and they plot far from the OIB and MORB fields. The second and third groups mainly plot in the OIB field. (d) Ba/Nb -La/Nb ratios: All samples from the three groups show approximately similar Ba/Nb ratios values but La/Nb ratios for HMB samples are less than those for the two other groups. This diagram shows that the HMB group is completely different and has no affinity with MORB or OIB but the two other groups another show some affinity with OIB. Symbols are the same as Fig.6. Ratios for the MORB/OIB, bulk silicate earth and upper continental crust are from [68–71]. Fields for MOIB/OIB and arc volcanism are compiled from [72].

lite sequence in this area. Also [21, 55] have considered the extension tectonic regime without the development of oceanic crust. Our new chemical and isotope data indicate that magmatic activity in the Mawat area has some affinity to OIB type and HMB rocks. Also, the chemical and isotope data confirm the mixing trend for group 2. The isotope ratios, REE trends and the quantities of major and trace elements do not confirm the MORB, island arc or supra- subduction zone as the magma sourcefor the Mawat area. Our findings do not support the role of slab fluids or crustal contamination for the source magma, or contamination during the upwelling of magma. But they show some affinity with a mantle plume from depth and contamination with some OIB-type magma. Furthermore, the high amount of MgO reflects the high degree of melting of the source mantle under high temperature and low-pressure conditions. The predominance of mafic rocks with high MgO and the distribution of different types of rocks in some sort of ring structure in the Mawat complex lead us to the conclusion that a hot spot or mantle plume is the source for the production and distribution of the voluminous magmatic rocks in this area. In order to provide context for our proposed model, we will briefly summarize previously described mantle plume models [37]. They proposed the three models for plumes from the different source as below (Fig. 11):

Model 1: mantle plume originates at 670 Km discontinuity entraining lower mantle in its core.
Model 2:; Start-up plume from D" layer with entrained lower mantle, passes through 670 km without significant development of a shell upper mantle.

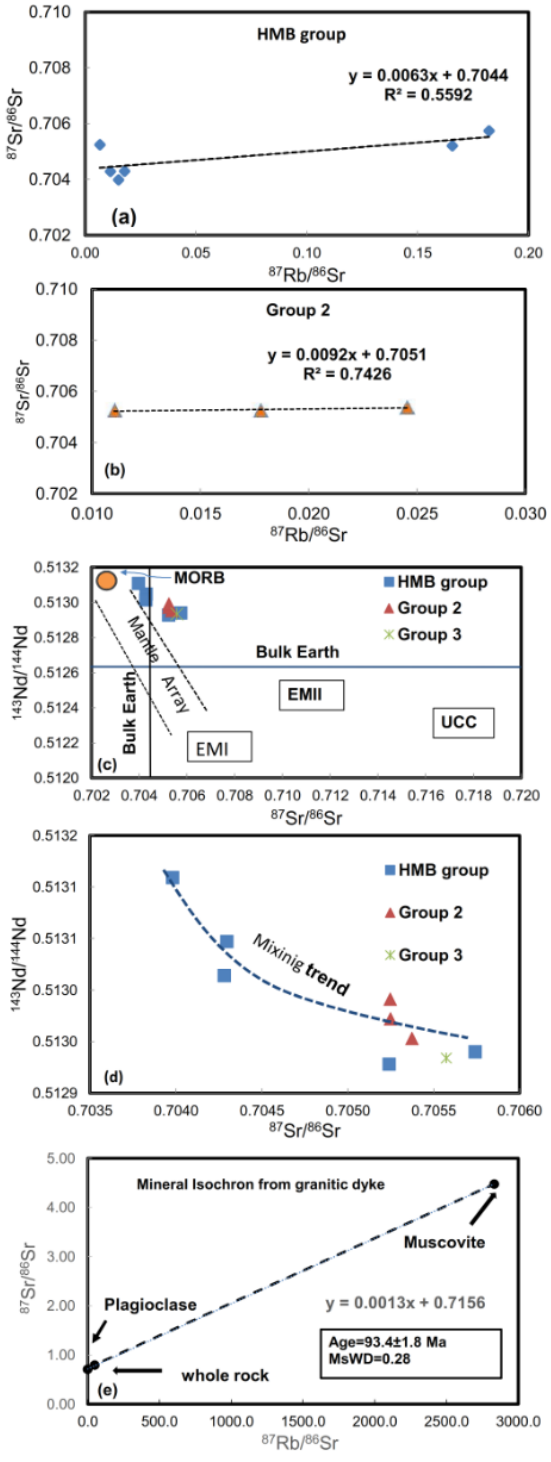

Figure 9. 87Rb/86Sr-87Sr/86Sr ratio diagram (a and b): shows the positive correlation for two groups in isochron diagram with 87Sr/86Sr initial ratios 0.7044 and 0.7051 for HMB and second group respectively.87Sr/86Sr- 143Nd/144Nd ratios diagram (c, d): Most of the samples plot in the depleted mantle field. The diagram shows a good mixing trend between the third and HMB groups for the development of the second group (d). Based on this diagram, the second group probably has developed from mixing of the third and HMB groups. The mineral isochrons for the granitic dyke shows an age of 92 Ma for the S- type granitic dyke (c). *The ages were calculated using ISOPLOTV3.71 [73] with* $\lambda = 1.42 \times 10 - 11y - 1$ *for Rb-Sr [74, 75]. UCC = upper Continental Crust [76].*

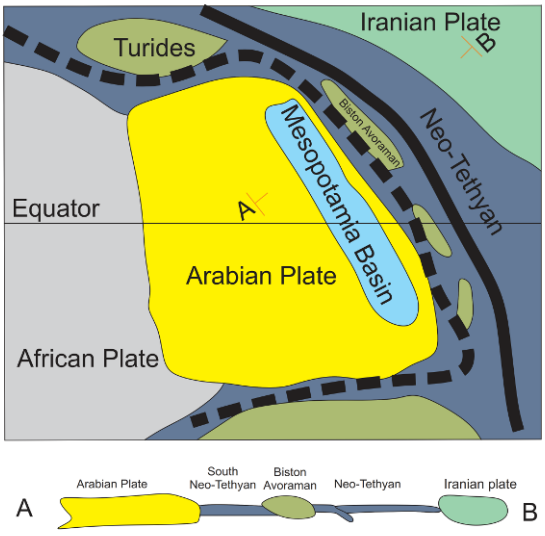

Figure 10. Simplified geodynamic map of the Arabian passive margin in the Mesozoic for extension of the Neo-Tethys branch along the eastern part of the Arabian Plate [65].

Model 3: Plume from the lower mantle stalls at 670 Km, heats the upper mantle, and creates a secondary mantle plume.

The dominance of HMB rocks in the Mawat complex suggests it is possible that these rocks have originated directly from a depleted mantle such as the D" layer. In this case, the upwelling of the mantle plume from the lower mantle or D" layer originates deep under the continental lithosphere, where the extensional regime facilitates the upwelling of the melt to shallower depths causing a high degree of partial melting. Accordingly, we propose the following model for the Mawat igneous complex:

The Iranian Plate started to drift away from the Arabian Plate in the Late Permian [56–58] and the Neo-Tethys oceanic crust developed during the Early Triassic, forming the Mesopotamian subsidence in the east of Iraq [21]. During the Middle to Late Triassic further extension occurred in the northern and eastern part of the Arabian passive margin. The occurrence of alkali basalts in Oman, Turkey and Zagros in this time span is good evidence for this extensional regime [59]. A discontinuous oceanic-type ridge developed parallel to the Neo-Tethys in the Arabian passive margin in the Middle to Late Jurassic time. The same model is proposed for Syria and Egypt [60]. The Mawat complex is the result of this extensional tectonic regime. Based on this interpretation, the emplacement of the mantle plume at lower depths during the Late Paleozoic was responsible for rifting of the Iranian section from the Arabian plate and for the opening of Neo-Tethys

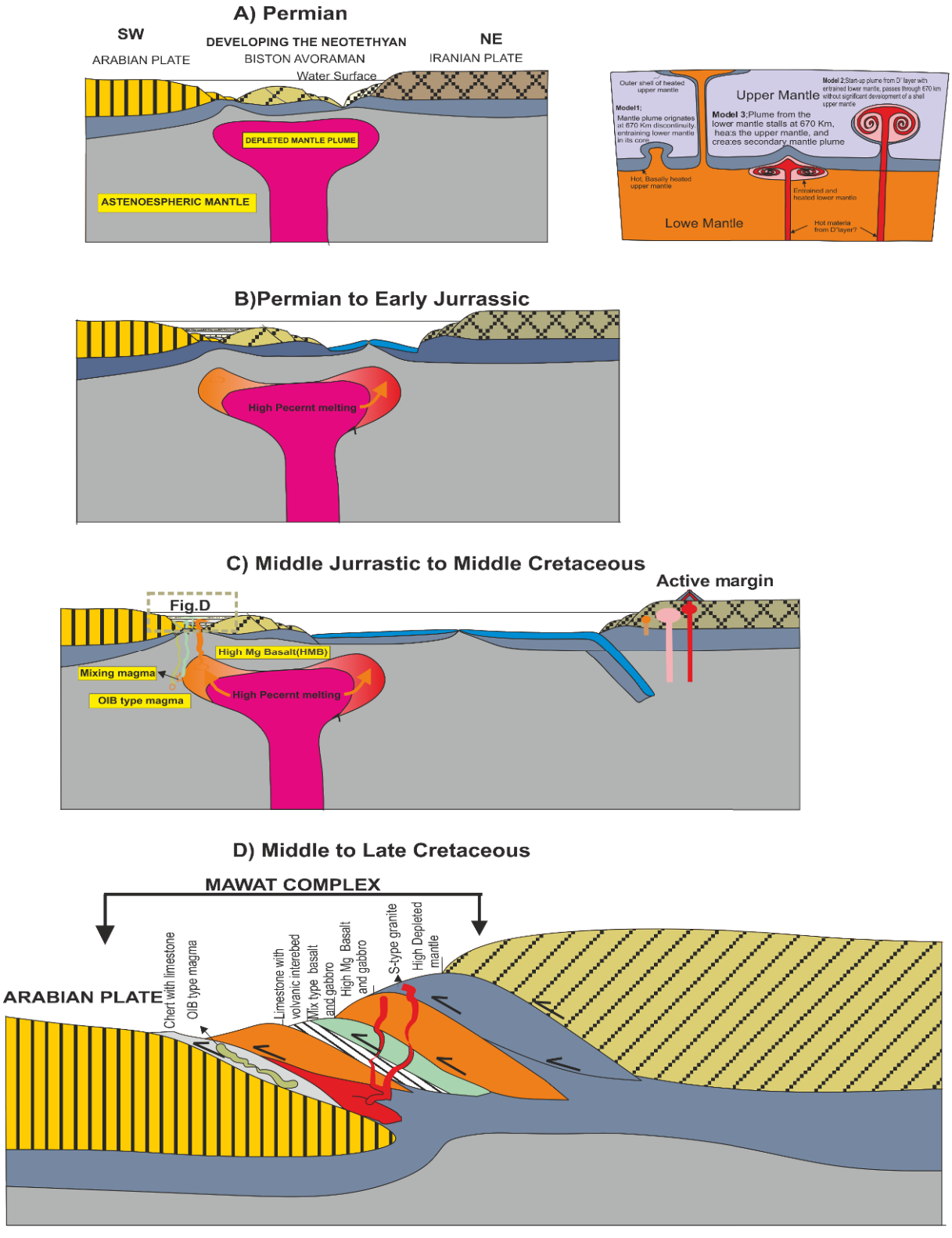

Figure 11. Tectonic model (a, b and c): The right (upper) shows the classical formation of three types of mantle plume with different sources. The model shows development of the Neo-Tethys oceanic crust between the Arabian and Iranian Plates and the parallel rifting in the Arabian passive margin during the mantle plume activity, which leads to the intrusions of three types of magma during the extensional regime in the passive margin. (d) Final stage: the collision of the Arabian passive margin with Biston-Avoraman block (BAB) in the Late Cretaceous and the squeezing of the Mawat complex between these two blocks followed by the formation of the S-type granites during the collision.

Ocean. At that time, because of the extensional tectonic regime some normal faults developed on the Arabian passive margin, causing the formation of extensional basins parallel to the Neo-Tethys oceanic ridge in the Arabian passive margin (Fig. 11a and b). This extension continued accompanied by the thinning of the continental lithosphere causing upwelling of the mantle plume, with significant melting below the Arabian passive margin. During the extensional tectonic regime, a graben-type basin was formed in Mawat area, accompanied by deposition of sediments, and volcanic activity such as OIB type magma intruded into this basin, hence, some OIB-type basaltic magma crystallized between the sedimentary layers. The absence of pillow structures and pelagic sediments indicates a relatively shallow water depth. In this case most of the OIB-type magmas have been concentrated in the rim of Mawat complex. With more extension significant melting of the mantle plume occurred and so the huge volumes of mafic magma were intruded into the Mawat basin. Some of the mafic magmas have crystallized at the base of the basin as coarse grained gabbro. This probably occurred in the Jurassic to Early Cretaceous. During the Late Cretaceous the Mawat complex was squeezed between the Arabian Plate and the Biston-Avoraman Block (BAB) and some granitic bodies have been intruded as dykes of few centimeters to few meters in width during this compression. These are S-type granites rich in K-feldspars, quartz, muscovite and tourmaline. The Rb-Sr mineral isochrones show an age of 93 Ma for these rocks (Fig. 9e), which corresponds with the Late Cretaceous collision in this area. During the collision, because of the thin lithosphere below the Mawat basin some residues of the depleted mantle such as dunite and harzburgite have been overthrust on the mafic complex. Overthrusting and deformation during the collision were accompanied by metamorphism, foliation and mylonitization. K-Ar and Ar-Ar dating show 107-95 Ma [61] for metamorphism in the Late Cretaceous. According to our model, the Mawat igneous complex is not produced by the obduction on the Arabian passive margin during Zagros Orogeny, because most recent works confirm that the collision between the Arabian and Iranian Plates occurred in the Late Miocene [30, 62–65]. During the collision between the Arabian and Iranian plates in the Late Miocene the Mawat complex was overthrust on the Red Bed Series.

8. Conclusion

The Mawat complex does not show a typical ophiolite sequence, and it is composed mainly of mafic rocks, which have been intruded into an extensional tectonic regime on the Arabian passive margin. It is possible that some extensional regime affected the passive margin of the Arabian Plate since the Late Paleozoic to the Late Mesozoic. Such extension caused thinning of the lithosphere such that hot depleted mantle-plume material was melted percent to a high degree.

9. Acknowledgements

This project was supported by Daiko Foundation No.10132 in Japan and JSPS KAKENHI Grant (No. 25303029). The authors thank the University of Kurdistan (Iran) and University of Baghdad (Iraq) for support during the field trips. This version has benefited from the anonymous reviewers, journal editor and Managing editor Katarzyna Cyran. We also would like to thank Prof. Kamal H. Karim in theDepartment of Geology, University of Sulaimaniye for his invitation to join the common project on the Mawat complex, Prof K. Yamamoto, M. Shimizu and H. Nagata from Nagoya University for their support in XRF and ICP-MS techniques. S. Razyani, A. Khani, M. Komailian, M. Shiri and F. Noori for their fieldwork and technical assistance.

References

[1] Anderson D.L., Isotopic evolution of the mantle: the role of magma mixing. Earth and Planetary Science Letters., 1982, 57, 1-12

[2] Morgan P., Baker, B.H., Introduction-processes of continental rifting. Tectonophysics., 1983, 94, 1-10

[3] Morgan, W.J., Convection plumes in lower mantle. Nature, 1971, 230, 42-43

[4] Davies H.L., Sun S.S., Frey F.A., Gautier I., McCulloch M.T., Price R.C., Bassias Y., Leclaire L., Basalt basement from the Kerguelen Plateau and the trail of a Dupal plume. Journal of Mineralogy and Petrology, 1989, 103, 457-469

[5] Griffiths R.W., Campbell I.H., Stirring and structure in mantle starting plumes. Earth and Planetary Science Letters., 1990, 99, 66-78

[6] Davies J.H., Bunge H.P., Are splash plumes the origin of minor hotspots? Geology., 2006, 34, 349-352

[7] Hawkesworth C., Scherstï£¡n A., Mantle plumes and geochemistry. Chemical Geology., 2007, 241, 319-331

[8] McKenzie D., Bickle M.J., The volume and composition of melt generated by extension of the lithosphere. Journal of Petrology., 1988, 29, 625-679

[9] King S.D., Anderson D.L., Edge-driven convection.

Earth and Planetary Science Letters., 1998, 160, 289-296.
[10] White R., McKenzie D., Magmatism at rift zones: the generation of volcanic continental margins and flood basalts. Journal of Geophysical Research., 1989, 94, 7685-7729
[11] Elkins-Tanton L.T., Hager B.H., Melt intrusion as a trigger for lithospheric foundering and eruption of the Siberian flood basalt. Geophysical Research Letters., 2000, 27, 3937-3940
[12] Elkins-Tanton L.T., Continent magmatism caused by lithospheric delamination. In: Foulger G.G., Natland J.H., Presnall D.C.,Anderson D.L. (Eds.), Plates, Plumes, and Paradigms. Geological Society of America Special Paper., 2005, 388, 449-462
[13] Miller G.H., Miller C.F., Tertiary extension-related volcanism, Old Woman Mountains area, eastern Mojave Desert, California. Journal of Geophysical Research., 1991, 96, 629-643
[14] Herzberg C., Depth and degree of melting of komatiites. Journal of Geophysical Research., 1992, 97, 4521-4540
[15] Nisbet E.G., Cheadle M.J., Arndt N.T., Bickle M.J., Constraining the potential temperature of the Archaean mantle: A review of the evidence from komatiites. Lithos., 1993, 30, 291-307
[16] Hoang N., Uto K., Geochemistry of Cenozoic basalts in the Fukuoka district (northern Kyushu, Japan): implications for asthenosphere and lithospheric mantle interaction. Chemical Geology., 2003, 198, 249-268
[17] Tang Y.J., Zhang H.F., Ying J.F., Asthenosphere-lithospheric mantle interaction in an extensional regime: Implication from the geochemistry of Cenozoic basalts from Taihang Mountains, North China Craton. Chemical Geology, 2006, 233, 309-327
[18] Chakrabarti R., Basu A.R., Basu A.R., Santo A.P., Tedesco D., Vaselli O., Isotopic and geochemical evidence for a heterogeneous mantle plume origin of the Virunga volcanics, Western rift, East African Rift system. Chemical Geology., 2009, 259, 273-289
[19] Starkey N.A., Fitton J.G., Stuart F.M., Larsen L.M., Melt inclusions in olivines from early Iceland plume picrites support high 3He/4He in both enriched and depleted mantle. Chemical Geology., 2012, 54, 306-307
[20] Bolton C.M.G., Geological Map, Kurdistan Series, scale 1: 100 000, Sheet K4, Rania. GEOSUR., int. rep., 1958, no. 276.
[21] Jassim S.Z., Goff J.C., Geology of Iraq. Dolin, Prague and Moravian Museum, Brno., 2006
[22] Al-Mehiadi, H., Geological investigation of Mawat, Chwarta area, NE Iraq. Unpublished report, SOM Library., 1975, No. 609
[23] Buday Y., Jassim S.Z., The regional Geology of Iraq, v.2: Tectonism,magmatism and Metamorphism. Geol.Min.Inv., Baghdad., 1987
[24] Al-Saadi A.J.H., Petrology and geochemistry of volcanic rocks in Northeastern Thrust Zone, NE-Iraq. Unpublished M.Sc Thesis, University of Baghdad., 1990
[25] Stocklin J., Structural history and tectonic of Iran; a review. Am. Assoc. Petroleum Geologists Bull., 1968, 52, 1229-1258
[26] Jassim S.Z., Geology of the central sector of the Mawat Igneous Complex, Northeastern Iraq. Jour. Geo. Soc. Iraq., 1972, 5, 83-92
[27] Al-Hassan M.I., Comparative petrologic study between Mawat and Penjwin Igneous Complexes, Northeastern Iraq. Unpublished M.Sc. Thesis, Baghdad University., 1975
[28] Allahyari K., Saccani E., Pourmoafi M., Beccaluva L., Masoudi F., Petrology of mantle pridotites and intrusive mafic rocks from the Kermanshah ophiolitic complex (Zagros belt, Iran). Implications for the geodynamic evolution of the Neo-Tethyan oceanic branch between Arabia and Iran. Ofioliti., 2010, 35, 71-90
[29] Azizi H., Chung S.L., Tanaka T., Asahara,Y., Isotopic dating of the Khoy metamorphic complex (KMC), northwestern Iran: A significant revision of the formation age and magma source. Precambrian Research., 2011a, 185, 87-94
[30] Azizi H., Tanaka T., Asahara Y., Chung S.L., Zarinkoub, M.H., Discrimination of the age and tectonic setting for magmatic rocks along the Zagros thrust zone, northwest Iran, using the zircon U-Pb age and Sr-Nd isotopes. Journal of Geodynamics., 2011b, 52, 304-320
[31] Saccani E., Allahyari K., Beccaluva L., Bianchini G., Geochemistry and petrology of the Kermanshah ophiolites (Iran): Implication for the interaction between passive rifting, oceanic accretion, and OIB-type components in the Southern Neo-Tethys Ocean. Gondwana Research., 2012, article in press
[32] Mohammad Y.O., Serpentines and their tectonic signature along the northwest Zagros thrust zone, Kurdistan Region, Iraq Arab. J. Geosciences., 2011, 4, 69-83, DOI 10.1007/s12517-009-0080-y
[33] Ismail S. A., Mirza T.M., Carr P.F., Platinum-group elements geochemistry in podiform chromitites and associated peridotites of the Mawat ophiolite, northeastern Iraq. Journal of Asian Earth Sciences., 2010, 37, 31-41
[34] Tanaka T., Togashi S., Kamioka H., Amakawa H., Kagami H., Hamamoto T., Yuhara M., et al., JNdi-1:

A neodymium isotopic reference in consistency with LaJolla neodymium. Chemical Geology., 2000, 168, 279-281

[35] Le Bas M.J., LeMaitre R.W., Streckeisen A., Zanettin B., A chemical classification of volcanic rocks based on the total alkali silica diagram. Journal of Petrology., 1986, 27, 745-750

[36] Sun S.S., McDonough W.F., Chemical and isotopic systematic of oceanic basalts: implication for mantle composition and processes. In: Sunders, A.D., Norry, M.J. (Eds.), Magmatic in Oceanic Basins, Special Publication 42. Geological Society of London., 1989, 313-345

[37] Fitton J.G., Saunders A.D., Norry M.J., Hardarson B.S., Taylor, R.N., Thermal and chemical structure of the Iceland plume. Earth and Planetary Science Letters., 1997, 153, 197-208

[38] Pearce J.A., Geochemical fingerprinting of oceanic basalts with applications to ophiolite classification and the search for Archean oceanic crust. Lithos., 2008, 100, 14-4

[39] Manikyamba C., Kerrich, R., Geochemistry of alkaline basalts and associated high-Mg basalts from the Penakacherla Terrane, Dharwar craton, India: An Archean depleted mantle-OIB array. Precambrian Research., 2011, 188, 104-122

[40] Zheng J.P., Griffin W.L., Reilly S.Y., Hu B.Q., Zhang M., Tang H.Y., Su Y.P., Zhang Z H., Pearson N., Wang F.Z., Lu F.X., Continental collision and accretion recorded in the deep lithosphere of central China. Earth and Planetary Science Letters., 2008, 269, 497-507

[41] Aswad K., Aziz N.R.H., Koyi H.A., Cr-spinel compositions in serpentinites and their implications for the petrotectonic history of the Zagros Suture Zone, Kurdistan region, Iraq. Geological Magazine., 2011, 148, 802-818

[42] Ali S.A., Geochemistry of Tethyan-Arc related volcanic rocks, NE Iraq (PhD. Thesis). Wollongong, NSW, Australia, University of Wollongong., 2012

[43] Ali S.A., Buckman S., Aswad K.J., Jones B.G., Ismail S.A., Nutman A.P., The tectonic evolution of a Neo?Tethyan (Eocene-Oligocene) island?arc (Walash and Naopurdan groups) in the Kurdistan region of the Northeast Iraqi Zagros Suture Zone. Island Arc., 2012, DOI: 10.1111/iar.12007

[44] Oweiss G.A., The Penjwin area, along the Zagros suture zone, as an example of collisional orogen. Tectonophysics, 1984, 101, 55-62

[45] Jassim S.Z., Geology of the central sector of the Mawat igneous complex, NE Iraq. Jour. Geol. Soc. Iraq., 1973, 6, 83-92

[46] Mashek J., Etabi W., Petrology of the Mawat Igneous-metamorphic complex. NIMCO Lib. Unpublished report., 1973

[47] Jassim S.Z., Al. Hassan M.I., Petrography and origin of the Mawat and Penjwin Igneous Complex: a comparison. Jour. Geol. Soc.Iraq, special issue., 1977, 169- 210

[48] Buda G., Al Hashimi W.S., Petrology of Mawat OphioliteComplex.Northeastren Iraq .Jour. Geol. Soc. Iraq., 1977, 10, 69-98

[49] Zekaria M.,B.,M., Petrology and geochemistry of the southern part of Mawat ophiolite complex, Northeastern Iraq, Unpublished Msc.Thesis, Mosul University., 1992 (in Arabic)

[50] Al-Samman A.H., Zekaria M.B., Younis, J.S., Geochemical variation of Mawat Ophiolite Volcanics, Waraz, NE Iraq. Raf. Jour.. 1996, Sci. 7, 55-67

[51] Aswad K.J., Arc-continent collision in northeastern Iraq as evidenced by Mawat and Penjween ophiolite complexes. Raf. Jour. Sci., 1999, 10, 51- 61

[52] Koyi A., Petrochemistry, petrogenesis and Isotope dating of Walash volcanic rocks at Mawat-Chowarta area, NE Iraq, Unpublished MSc.Thesis, Universty of Mosul., 2006, 230p. (In Arabic)

[53] Farjo, S.F., Geochemistry and petrogenesis of the volcanic rocks of Mawat ophiolite complex, NE-Iraq, Unpublished MSc. Thesis, University of Mosul.,2006 (in Arabic).

[54] Numan N.M.S., Major Cretaceous Tectonic Events in Iraq. Raf. Jour. Sci., 2000, 11, 32-52

[55] Karim A., Berkhli M., et al., Le Visï£¡en supï£¡rieur d'Azarhare (Maroc central): environnements de dï£¡pï£¡t, datation et ï£¡volution diagï£¡nï£¡tique. Comptes Rendus Geoscience., 2005, 337, 525-532

[56] Ricou L.E., Tethys reconstructed plate's continental fragments and their boundaris since 260 Ma from Central America to South-eastern Asia. Geodinamica Acta., 1994, 7, 169-218

[57] Stampfli G.M., Tethyan oceans. Geological Society Special Publication., 2000, 173, 1-23

[58] Garfunkel Z., Origin of the Eastern Mediterranean basin: a reevaluation. Tectonophysics., 2004, 391, 11-34

[59] Pillevuit A., Marcoux J., et al., The Oman exotics: a key to the understanding of the Neotethyan geodynamic evolution. Geodinamica Acta., 1997, 10, 209-238

[60] Brew D.S., Late Weichselian to early Holocene subaqueous dune formation and burial off the North Sea Northumberland coast. Marine Geology, 134., 1996, 203-211

[61] Aswad K.J., Elias E.M., Petrogenesis, Geochemistry,

and Metamorphism of spilitized subvolcanic rocks of the Mawat Ophiolite Complex, NE Iraq. Ofiolitti., 1988, 13, 95-109

[62] Agard P., Omrani J., Jolivet L., Mouthereau F., Convergence history across Zagros (Iran): constraints from collisional and earlier deformation. Geologische Rundschau., 2005, 94, 401-419

[63] Azizi H., Moinevaziri H., Review of the tectonic setting of Cretaceous to Quaternary volcanism in northwestern Iran. Journal of Geodynamics., 2009, 47, 167-179

[64] Agard P., Omrani J., Jolivert L., Whitechurch H., Vrielynck B, Spakman W., Monie P., Meyer B., Wortel R., Zagros orogeny: A subduction-dominated process. Geological Magazine., 2011, 148, 692-725

[65] Verdel C., Wernicke B. P., Hassanzadeh J., Guest B., A Paleogene extensional arc flare-up in Iran. Tectonics., 2011, 30 (3), TC3008. http://dx.doi.org/10.1029/2010TC002809

[66] Buday T., The regional geology of Iraq, Stratigraphy and paleogeography. Edited by Kassab, I.M. and Jassim S.Z., Dar Al- Kutib publishing house, Mosel, Iraq., 1980

[67] Passchier C.W., Trouw, R.A.J., Microtectonis, Springer Verlag., 2005

[68] Hofmann A.W., Jochum K.P., Seufert M., White W.M., Nb and Pb in oceanic basalts: new constraints on mantle evolution. Earth and Planetary Science Letters., 1986, 79, 33-45

[69] McDonough W.F., Stosch H.G., et al., Distribution of titanium and the rare earth elements between peridotitic minerals. Contributions to Mineralogy and Petrology., 1992, 110, 321-328

[70] McDonough W.F., Sun, S.S., The composition of the Earth. Chemical Geology., 1995, 120, 223-253

[71] Rudnick R.L., Fountain D.M., Nature and composition of the continental crust: A lower crustal perspective. Reviews of Geophysics., 1995, 33, 267-309

[72] Chung S.L., Wang K.L., Crawford A.J., Kamenetsky V.S., Chen C.H., Lan C.Y., Chen, C.H., High-Mg potassic rocks from Taiwan: implications for the genesis of orogenic potassic lavas. Lithos., 2001, 59, 153-157

[73] Ludwig K.R., ISOPLOT: a plotting and regression program for radio-isotope data. U.S. Geol. Survey Open-File Report., 2009, 91-445

[74] Steiger R.H., Jager E., Subcommission on geochronology: convention on the use decay constants in geo- and cosmochronology. Earth and Planetary Science Letters., 1977, 36, 359-362

[75] Begemann, F., Kudwig K.R., Lugmair, G.W., Min K., Nyquist L.E., Patchett, P.J., Ben Othman D., White W.M., et al., 1989. The geochemistry of marine sediments, island arc magma genesis, and crust-mantle recycling. Earth and Planetary Science Letters., 1989, 94, 1-21

[76] Taylor S.R., McLennan S.M., The Continental Crust: its Composition and Evolution. An Examination of the Geochemical Record Preserved in Sedimentary Rocks. The Continental Crust: its Composition and Evolution. Blackwell., 1985